ELSEVIER

#### Contents lists available at ScienceDirect

# Aerospace Science and Technology

journal homepage: www.elsevier.com/locate/aescte



# Resilient multi-UAS coordination using cooperative localization



Harshvardhan Uppaluru, Hamid Emadi, Hossein Rastgoftar\*

Scalable Move And Resilient Traversability (SMART) Lab, Aerospace and Mechanical Engineering Department, University of Arizona, Tucson, AZ, USA

#### ARTICLE INFO

Article history:
Received 17 April 2022
Received in revised form 8 September 2022
Accepted 17 October 2022
Accidable online 25 October 2022
Communicated by Tsourdos Antonios

Keywords: Unmanned aerial systems (UAS) Multi-UAS (MUS) State estimation Continuum deformation coordination

#### ABSTRACT

Over the last decade, Multi-UAS system (MUS) have found a variety of applications such as surveillance, data acquisition, search and rescue, and delivery tasks in various environments. However, for reliable operation of MUS, it is critical to provide safety guarantee conditions assuring obstacle collision avoidance, as well as, inter-UAS collision avoidance. In this work, we apply the principles of continuum mechanics to develop a physics-inspired algorithm to ascertain safe and resilient operation of a MUS in the presence of disturbances and unforeseen UAS failure(s). In particular, the proposed approach consists of two modes: (i) Homogeneous Deformation Mode (HDM), and (ii) Failure Resilient Mode (FRM). We formally specify transitions between HDM and FRM using Cooperative Localization (CL) approach to quantify UAS tracking error and detect anomalous conditions due to UAS failure.

© 2022 Elsevier Masson SAS. All rights reserved.

#### 1. Introduction

Unmanned Aerial Systems (UAS) have found a variety of academic and industrial applications such as small package delivery [1], autonomous sensing [2], data acquisition from hazardous environments [3] or agricultural farm fields [4], aerial surveillance [5,6], urban search and rescue [7], wildlife monitoring and exploration [8], and urban traffic monitoring [9] over the past decade. Multi-UAS System (MUS) is a low-cost system with the capability of performing complex tasks that require high controllability and agility. However, to leverage the capabilities of a MUS, effective decentralized coordination and path planning approaches, that are resilient to UAS failure are needed. The main goal of this paper is to develop a physics-inspired algorithm ensuring safety of large-scale UAS coordination in the presence of unexpected actuation failure/s.

## 1.1. Related work

Localization of an Unmanned Aerial System (UAS) team has been a challenging problem for researchers [10]. GPS-based coordination [11,12], Simultaneous Localization And Mapping (SLAM) [13] and embedded beacon-based localization algorithms [14], which rely on GPS signals or existence of static landmarks, are the

E-mail addresses: huppaluru@arizona.edu (H. Uppaluru), hamidemadi@arizona.edu (H. Emadi), hrastgoftar@arizona.edu (H. Rastgoftar).

available MUS localization approaches. GPS-based localization can have major drawbacks because UAS relying on GPS-based localization may experience cybernetic attacks by malicious UAS [15]. Furthermore, it may not effectively work for position estimation of multiple UAS coordinating in GPS-denied environments. To overcome these issues, researchers have applied Cooperative Localization (CL) approaches [16,10] to estimate global positions of the MUS by processing local position information collected from individual UAS in a distributed fashion. Available CL approaches can be classified into centralized [17] and decentralized [18] methods, and applied by the available decentralized multi-UAS coordination techniques, such as Consensus [19,20], Containment Control [21], Partial Differential Equation (PDE)-based methods [22], Continuum Deformation [23-25], and Graph Rigidity [26], to localize UAS and estimate their global positions in the presence of noise and disturbances. For state estimation in the presence of disturbances modeled by Gaussian Processes (GP), existing CL methods have implemented various approaches such as Extended Kalman filters (EKFs) [27],[28]; maximum likelihood [29], maximum a posteriori (MAP) [18], and particle filters [30]. Also, authors in [31] present a CL technique to deal with systems under non-Gaussian noises.

Sense And Avoid (SAA) is an existing algorithm proposed for collision avoidance of UAS in case of pop-up failures or unexpected situations [32]. Authors in [33] proposed a collision avoidance method based on estimating and predicting the UAS trajectory. A reference SAA system architecture based on Boolean Decision Logics was presented in [34]. Authors in [35] provided a complete survey on SAA technologies in the sequence of fundamental func-

<sup>\*</sup> Corresponding author.

tions/components of SAA in sensing techniques, decision making, path planning, and path following.

### 1.2. Contributions and outline

This paper develops a physics-inspired solution for faultresilient multi-UAS (MUS) coordination. To assure safety and resilience of the MUS, we propose an approach with two operation modes: (i) Homogeneous Deformation Mode (HDM) and (ii) Failure-Resilient Mode (FRM). In HDM, active UAS are all healthy and considered as a finite number of particles of a 2-D deformable body moving collectively in a 3-D motion space. The desired coordination of the MUS is defined by an affine transformation with non-singular lacobian matrix which is called homogeneous transformation in continuum mechanics. In FRM, the MUS has at least 1 failed UAS that cannot follow the desired group coordination. Therefore, MUS are classified as healthy and failed UAS, and the desired trajectories of the healthy UAS are planned such that the failed UAS are safely wrapped and excluded from the shared motion space. More specifically, healthy UAS are treated as particles of an ideal fluid flow wrapping the failed UAS considered as singularities in the motion space. Compared to the corresponding author's previous work [36], this paper offers the following novel contributions:

- 1. We apply the cooperative localization approach to quickly detect UAS failures in the presence of noise and disturbances only by filtering the relative position information.
- 2. We specify transition conditions from HDM to FRM by using the cooperative localization.
- 3. We propose a novel approach for generation of the localization graph every time FRM is transitioned to HDM once the failed UAS leave the group of the healthy UAS.
- 4. While Ref. [36] assumes that the total number of failed UAS remains unchanged at FRM, this restriction is relaxed in this paper by authorizing multiple UAS failures that can occur at different times when FRM is active.
- 5. While Ref. [36] assumes that the total number of failed UAS remains inside a stationary containment domain, we develop a fault resilient multi-UAS coordination model in the presence of time-varying failed UAS.

This paper is organized as follows: Preliminaries and Assumptions are given in Section 2. Problem Statement is discussed in Section 3. Our approach for fault-resilient multi-UAS coordination is presented in Section 4. Simulation results are presented in Section 5 and followed by concluding remarks in Section 6.

#### 2. Preliminaries

Consider a MUS with n UAS in a 3-D motion space, where UAS are identified by the set  $\mathcal{V}=\{1,\cdots,n\}$ . We use the following notations throughout this paper:  $\mathbf{r}_i(t)$ ,  $\mathbf{r}_{i,d}(t)$  and  $\hat{\mathbf{r}}_i(t)$  denote the global position, desired position and estimated position of UAS  $i\in\mathcal{V}$  in the global Euclidean coordinate system at time t, respectively.

Set  $\mathcal{V}$  is divided into two disjoint subsets  $\mathcal{V}_A$  and  $\mathcal{V}_I$ , which represent the *active* and *inactive* UAS, respectively (i.e.  $\mathcal{V} = \mathcal{V}_A \bigcup \mathcal{V}_I$ ). Active UAS, identified by set  $\mathcal{V}_A$ , are the cooperative UAS admitting the desired continuum deformation coordination. They are enclosed by a ball  $\mathcal{C}_0(\bar{\mathbf{r}}_h, \rho_0)$  where  $\bar{\mathbf{r}}_h$  is the centroid of all healthy UAS (see Fig. 1), given by  $\bar{\mathbf{r}}_h = \frac{1}{n_h} \sum_{j=1}^{n_h} \mathbf{r}_j(t)$  and  $\rho_0$  is the proper radius for  $\mathcal{C}_0$  such that all healthy UAS are enclosed. On the other hand, inactive UAS are the UAS located outside the ball  $\mathcal{C}_0(\bar{\mathbf{r}}_h, \rho_0)$ . The set of *inactive* UAS is denoted by  $\mathcal{V}_I$  and defined as  $\mathcal{V}_I = \mathcal{V} \setminus \mathcal{V}_A$ .

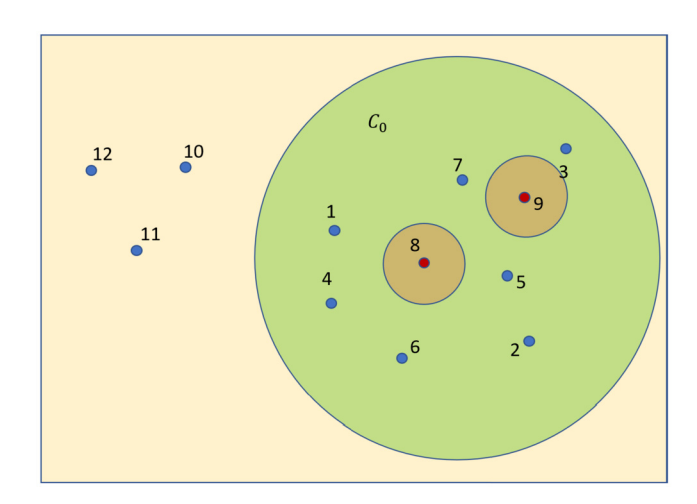


**Fig. 1.** An example of multi-UAS (MUS) containing 12 UAS. Green area represents  $C_0$ . All UAS in  $C_0$  are active, whereas the UAS outside the green area are inactive UAS. UAS located in a red circle are failed UAS. (For interpretation of the colors in the figure(s), the reader is referred to the web version of this article.)

**Definition 1.** An active UAS is *healthy*, if the corresponding sensors and actuators work accurately, and it is able to track the desired trajectory within a predefined tracking error. The set of healthy UAS is denoted by  $\mathcal{V}_H = \{i_1, \ldots, i_{n_h}\}$ , where  $n_h$  denotes the number of healthy UAS.

**Definition 2.** An active UAS is called a *failed* UAS, if its actuators do not work accurately, and therefore, it is not able to track the desired trajectory within the predefined tracking error. The set of failed UAS is defined by  $\mathcal{V}_F = \{i_1, \ldots, i_{n_f}\} = \mathcal{V}_A \setminus \mathcal{V}_H$ , where  $n_f$  denotes the number of failed UAS.

For the MUS shown in Fig. 1,  $\mathcal{V}_A = \{1, \ldots, 9\}$ ,  $\mathcal{V}_H = \{1, \ldots, 7\}$ ,  $\mathcal{V}_F = \{8, 9\}$  and  $\mathcal{V}_I = \{10, 11, 12\}$  at a specific time with two failed UAS. Let  $n_a(t)$  and  $n_i(t)$  denote the cardinality of  $\mathcal{V}_A$  and  $\mathcal{V}_I$  at time t, respectively. Note that  $\mathcal{V}_A$  and  $\mathcal{V}_I$  are time-varying sets, and  $n_a(t) + n_i(t) = n$ . In the system shown in Fig. 1  $n_a = 9, n_i = 3, n_b = 7, n_f = 2$ .

Next, we review the basics of graph theory, homogeneous deformation coordination, and ideal fluid flow coordination in Sections 2.1, 2.2, and 2.3, respectively.

## 2.1. Graph theory notations

We define a directed graph  $\mathcal{G}(\mathcal{V}_A(t),\mathcal{E}(t))$ , where  $\mathcal{V}_A(t)$  is the node set, and the edge set  $\mathcal{E}(t)\subseteq\mathcal{V}_A(t)\times\mathcal{V}_A(t)$  is defined as a set of pairs (i,j) connecting node i to node j  $(i,j\in\mathcal{V}_A(t))$ . If  $(i,j)\in\mathcal{E}(t)$ , then, UAS  $i\in\mathcal{V}_A(t)$  can measure the relative position of UAS  $j\in\mathcal{V}_A(t)$  at time t. If  $(i,i)\in\mathcal{V}_A(t)$ , then, UAS  $i\in\mathcal{V}$  is able to use GPS to localize itself with respect to the global coordinate system at time t.

The set of in-neighbor UAS for  $i \in \mathcal{V}_A$  is defined by  $\mathcal{N}_i(t) = \{j | (j,i) \in \mathcal{E}(t)\}$ . We consider  $\mathcal{G}(\mathcal{V}_A(t),\mathcal{E}(t))$  as a proximity-based graph in which  $\mathcal{N}_i(t)$  defines k-nearest UAS to UAS  $i \in \mathcal{C}$ . Without loss of generality, we choose k = 3, therefore,  $|\mathcal{N}_i| = 3$ ,  $\forall i \in \mathcal{V}_A$ .

#### 2.2. Homogeneous deformation coordination

We apply homogeneous deformation coordination approach [23] to plan the desired coordination of active UAS when  $\mathcal{V}_F(t) = \emptyset$  at time t. Three active UAS located at the vertices of a triangle, defined by set  $\mathcal{L} = \{l_1, l_2, l_3\}$ , are considered as leader UAS. The rest of  $(n_a - 3)$  UAS are considered as followers and are defined by set

 $\mathcal{F} = \mathcal{V}_A \setminus \mathcal{L} = \{l_4, \dots, l_{n_a}\}$ . Under homogeneous deformation coordination, the desired trajectory of each UAS  $i \in \mathcal{L}$  is defined with the following linear transformation [23]:

$$\mathbf{r}_{i,d}(t) = \mathbf{Q}(t,t_0) \left( \mathbf{r}_{i,0} - \mathbf{d}(t_0) \right) + \mathbf{d}(t) \quad t \in [t_0, t_f]$$
(1)

where  $\mathbf{Q}(t,t_0) \in \mathbb{R}^{3 \times 3}$  is the Jacobian matrix,  $\mathbf{r}_{i,0} = \begin{bmatrix} x_{i,0} & y_{i,0} & 0 \end{bmatrix}^T$  is the reference position,  $\mathbf{r}_{i,d}(t) = \begin{bmatrix} x_{i,d}(t) & y_{i,d}(t) & z_{i,d}(t) \end{bmatrix}^T$  and  $\mathbf{d}(.) \in \mathbb{R}^3$  is the rigid body displacement vector [37]. Since (1) is a linear transformation, followers' desired trajectories can be expressed as a weighted summation of the leaders' desired trajectories. For every UAS  $i \in \mathcal{F}$ , we define three parameters  $\alpha_{i,1}$ ,  $\alpha_{i,2}$ , and  $\alpha_{i,3}$  such that  $\sum_{j=1}^3 \alpha_{i,j} = 1$ .  $\alpha_{i,1}$ ,  $\alpha_{i,2}$ , and  $\alpha_{i,3}$  can be computed from the reference position of UAS i and the leaders' reference positions as follows:

$$\begin{bmatrix} \alpha_{i,1} \\ \alpha_{i,2} \\ \alpha_{i,3} \end{bmatrix} = \begin{bmatrix} x_{1,0} & x_{2,0} & x_{3,0} \\ y_{1,0} & y_{2,0} & y_{3,0} \\ 1 & 1 & 1 \end{bmatrix}^{-1} \begin{bmatrix} x_{i,0} \\ y_{i,0} \\ 1 \end{bmatrix}, \quad \forall i \in \mathcal{F}.$$
 (2)

The collective motion, under the homogeneous deformation coordination, is defined as a leader-follower problem in which the desired trajectory of UAS  $i \in \mathcal{F}$ , denoted by  $\mathbf{r}_{i,d}$ , can be written as

$$\mathbf{r}_{i,d}(t) = \sum_{j \in \mathcal{L}} \alpha_{i,j} \mathbf{r}_{j,d}(t), \quad \forall i \in \mathcal{F}.$$
 (3)

#### 2.3. Physics-based model properties

In the presence of failed UAS, when  $V_F \neq \emptyset$ , we treat healthy UAS as particles of an ideal fluid flow, defined by combining uniform and doublet flow patterns in the x-y plane [38,25]. To this end, we use complex variable  $\mathbf{z} = x + \mathbf{i}y$  to denote the position in the x-y plane, and obtain the potential function  $\Phi(x, y, t)$  and stream function  $\Psi(x, y, t)$  of the ideal fluid flow field by defining,

$$f(\mathbf{z},t) := \Phi(x, y, t) + \mathbf{i}\Psi(x, y, t)$$

$$= u_{\infty} \sum_{h \in \mathcal{V}_{n}} \left( \mathbf{z} - \mathbf{z}_{h}(t) + \frac{a_{h}^{2}}{\mathbf{z} - \mathbf{z}_{h}(t)} \right)$$
(4)

over the complex plane **z**, where  $\mathbf{z}_h(t)$  denotes the x, y components of position of the failed UAS. In (4),  $u_\infty$  and  $a_h$  are constant design parameters for planning the safety recovery trajectory.

Using the ideal fluid flow model, x and y components of every healthy UAS  $i \in \mathcal{V}_H$  are constrained to slide along the stream curve  $\Psi_i = \Psi(x_i(t), y_i(t))$  at any time  $t \geq t_0$ , where  $t_0$  is the reference time when at least one failed UAS is detected. Therefore, every failed UAS is excluded from the motion space by a cylinder elongated in z direction.

**Remark 1.** If  $n_f = 1$ , then, the cross-section of the wrapping cylinder is a circle of radius  $a_h$  centered at  $\mathbf{z}_h$ . Otherwise (i.e.  $|\mathcal{V}_F| > 1$ ), the cross sections of each cylinder enclosing a failed UAS is not an exact circle.

Equation (4) specifies a conformal mapping between the x-y and  $\Phi-\Psi$  planes, where  $\Phi(x,y,t)$  and  $\Psi(x,y,t)$  satisfy the Cauchy-Riemann conditions and Laplace partial differential equation at any time t:

$$\nabla^2 \Psi = 0, \quad \nabla^2 \Phi = 0, \quad \forall t. \tag{5}$$

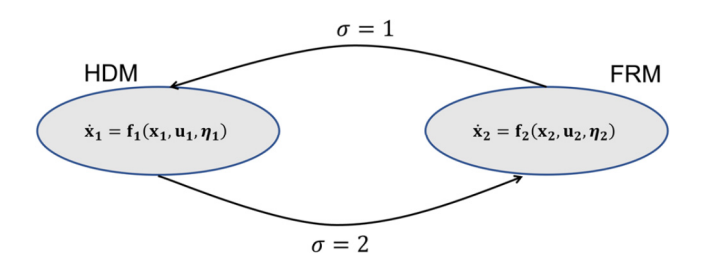


Fig. 2. The proposed hybrid system for fault resilient UAS coordination.

#### 3. Problem statement

In this paper, we consider the collective motion of a MUS in compact 3-D airspace denoted by  $\mathcal{C}$ . We aim to develop a model for multi-UAS coordination that is safe and resilient to UAS failure, and enables UAS to compute and track desired trajectories autonomously in the presence or absence of UAS failure. More specifically, the paper defines safety and resilience as follows:

- The multi-UAS coordination is defined as safe, if collision between every two UAS is avoided.
- The multi-UAS coordination is defined as resilient, if its' healthy UAS can continue their operation in the presence of sudden pop-up UAS failure/s.

To this end, we design a hybrid model to enable the interaction between the physical continuous dynamics and the rules of discrete switching logic. The state of the hybrid system is described by a combination of a continuous state variable  $\mathbf{x} \in \mathbb{R}^{n_x}$ , and a discrete state variable  $\sigma \in \mathcal{I} = \{1,2\}$  which describes the two different operating modes of the hybrid system.  $\sigma = 1$  and  $\sigma = 2$  correspond to the homogeneous deformation mode (HDM) and fault resilient mode (FRM), respectively (see Fig. 2).

HDM is active when there is no failed UAS detected and reported to the system, and all active UAS are healthy (i.e.  $\mathcal{V}_A = \mathcal{V}_H$  and  $\sigma = 1$ ). In this mode, UAS are considered as particles of a 2-D deformable formation in a 3-D motion space and cooperative coordination is performed by homogeneous deformation coordination presented in Section 2.2. Once a failed UAS is detected,  $\mathcal{V}_F \neq \emptyset$  and therefore, triggers a jump from  $\sigma = 1$  to  $\sigma = 2$  and switches the system to FRM. In FRM, we use the ideal fluid flow model, introduced in Section 2.3 to safely plan the coordination of the healthy UAS in the presence of failed UAS.

The transitions between HDM and FRM are operated safely by planning the group coordination in a centralized manner. To this end, we enable every healthy UAS  $i \in \mathcal{V}_H$  to measure relative positions of its in-neighbor UAS and report them to a commander UAS which is assigned based on the proximity to the centroid of the configuration of the healthy UAS using the approach presented in [36]. The commander UAS is responsible for detecting failures and decision making for switching the modes. Moreover, we assume that UAS are not deceptive; i.e. we do not consider the stealth attack scenarios. In our model, disturbance is the only source of uncertainty. These can be formally expressed as following assumptions.

Under the aforementioned model, we investigate the following problems:

**Problem 1.** We develop an algorithm based on HDM to acquire the desired coordination of all UAS through direct communication with leaders while the collision avoidance is assured. MUS coordination should be planned such that leaders and followers track the desired trajectories obtained from (1) and (3), respectively, when HDM is active (i.e.  $\mathcal{V}_A = \mathcal{V}_H$ ).

**Problem 2.** We develop an algorithm to detect anomalous conditions, and realize the set of failed UAS defined by  $\mathcal{V}_F$ . Our proposed approach operates between HDM and FRM automatically by only estimating the state vector of the system.

**Problem 3.** We develop an algorithm based on FRM to recover from the unsafe conditions and switch to HDM once the safety is recovered. When system is switched to FRM, all active UAS should compute the corresponding desired trajectories based on the ideal fluid flow model explained in Section 2.3.

**Remark 2.** While HDM can safely plan n-D ( $n \in \{1, 2, 3\}$ ) deformation, the FRM treats UAS as particles of 2-D ideal fluid flow coordinating in a 3-D motion space. As a result, when FRM is directed to restore the safety of the healthy UAS group coordination by having the faulty UAS leave the containment domain  $C_0$ , the desired z components of the healthy UAS remain time-invariant (in a 3-D motion space).

#### 4. Methodology

Consider an airspace C with a group of n UAS which lie in a closed set  $C_0$ , where the dynamics of each active UAS  $i \in \mathcal{V}_A$ , is modeled by

$$\dot{\mathbf{x}}_i = \mathbf{f}_i(\mathbf{x}_i) + \mathbf{g}_i(\mathbf{x}_i)\mathbf{u}_i + \eta_i. \tag{6}$$

In Eq. (6),  $\mathbf{x}_i \in \mathbb{R}^{n_x}$  is the state vector of UAS  $i \in \mathcal{V}_A$ ,  $\mathbf{f}_i(\mathbf{x}_i) : \mathbb{R}^{n_x} \to \mathbb{R}^{n_x}$ ,  $\mathbf{g}_i(\mathbf{x}_i) : \mathbb{R}^{n_x} \to \mathbb{R}^{n_x \times m_u}$  and  $\mathbf{u}_i \in \mathbb{R}^{m_u}$  is the control input vector of the system for UAS  $i \in \mathcal{V}_A$ .  $\eta_i$  is a process noise assumed to be a zero-mean independent Gaussian process with known covariance  $\mathbf{F}_i$ . The collective dynamics of this system can be expressed by

$$\dot{\mathbf{x}} = \mathbf{f}(\mathbf{x}) + \mathbf{g}(\mathbf{x})\mathbf{u} + \eta, \tag{7}$$

where

$$\mathbf{x} = \begin{bmatrix} \mathbf{x}_{1} \\ \vdots \\ \mathbf{x}_{n_{a}} \end{bmatrix}, \quad \mathbf{f} = \begin{bmatrix} \mathbf{f}_{1} \\ \vdots \\ \mathbf{f}_{n_{a}} \end{bmatrix}, \quad \mathbf{u} = \begin{bmatrix} \mathbf{u}_{1} \\ \vdots \\ \mathbf{u}_{n_{a}} \end{bmatrix},$$

$$\eta = \begin{bmatrix} \eta_{1} \\ \vdots \\ \eta_{n_{a}} \end{bmatrix}, \quad \mathbf{g} = \operatorname{diag} \left( \begin{bmatrix} \mathbf{g}_{1} \\ \vdots \\ \mathbf{g}_{n_{a}} \end{bmatrix} \right)$$
(8)

We assume that leaders have access to GPS measurements and they can measure their global positions. However, a follower  $i \in \mathcal{F}$  only measures the relative positions of its in-neighbors defined by  $\mathcal{N}_i$ . Assuming  $i \in \mathcal{V}_A$  has three in-neighbors,  $\mathcal{N}_i$  can be expressed by  $\mathcal{N}_i = \{i_1, \cdots, i_3\}$ , and

$$\mathbf{y}_i = \mathbf{h}_i(\mathbf{x}_i, \mathbf{x}_{i_1}, \cdots, \mathbf{x}_{i_3}) + \epsilon_i \tag{9}$$

assigns the relative positions of in-neighbors of  $i \in \mathcal{V}_A$ , where

$$\mathbf{h}_i: \mathbb{R}^{n_\chi} \times \mathbb{R}^{n_\chi} \to \mathbb{R}^{n_y}$$

is a smooth function, and  $\epsilon_i$  is the measurement noise, defined as a zero-mean independent Gaussian process with known covariances  $\mathbf{R}_i$ . Let  $\mathbf{y} = \begin{bmatrix} \mathbf{y}_1^T & \dots & \mathbf{y}_{n_a}^T \end{bmatrix}^T$  denote the collective measurement of the system. Therefore,

$$\mathbf{y} = \mathbf{h}(\mathbf{x}) + \epsilon \tag{10}$$

where

$$\epsilon = \begin{bmatrix} \epsilon_1 \\ \vdots \\ \epsilon_{n_a} \end{bmatrix}, \quad \mathbf{h} = \begin{bmatrix} \mathbf{h}_1 \\ \vdots \\ \mathbf{h}_{n_a} \end{bmatrix}. \tag{11}$$

In this work, we use the Extended Kalman Filter (EKF) state estimation algorithm following [39] to localize UAS with respect to the inertial coordinate system by processing the relative position measurements reported to the commander UAS. In the first step, we initialize the system as follows:

$$\hat{\mathbf{x}}(t) = \mathbb{E}[\mathbf{x}(t)] \tag{12}$$

$$\mathbf{P}(t) = \mathbb{E}[(\mathbf{x}(t) - \hat{\mathbf{x}}(t))(\mathbf{x}(t) - \hat{\mathbf{x}}(t))^T]$$
(13)

where  $\hat{\mathbf{x}}(t)$  and  $\mathbf{P}(t)$  refer to the predicted state estimate and predicted covariance estimate at time t, respectively.  $\mathbb{E}[\mathbf{x}(t)]$  is the expected value of random variable  $\mathbf{x}(t)$ . Executing the EKF [39] leads to the following state estimation equations.

$$\dot{\hat{\mathbf{x}}}(t) = \mathbf{f}(\hat{\mathbf{x}}) + \mathbf{g}(\hat{\mathbf{x}})\mathbf{u} + \mathbf{K}(\mathbf{y} - \mathbf{h}(\hat{\mathbf{x}}, t))$$
(14)

$$\mathbf{K} = \mathbf{P}\mathbf{H}^{\mathrm{T}}\mathbf{R}^{-1} \tag{15}$$

$$\dot{\mathbf{P}} = \mathbf{AP} + \mathbf{PA}^T + \mathbf{Q} - \mathbf{PH}^T \mathbf{R}^{-1} \mathbf{HP}$$
 (16)

where  $\mathbf{A} = \frac{\partial \mathbf{f}}{\partial \mathbf{x}}\Big|_{\hat{\mathbf{x}}}$  and  $\mathbf{H} = \frac{\partial \mathbf{h}}{\partial \mathbf{x}}\Big|_{\hat{\mathbf{x}}}$ .

#### 4.1. Coordination planning at HDM

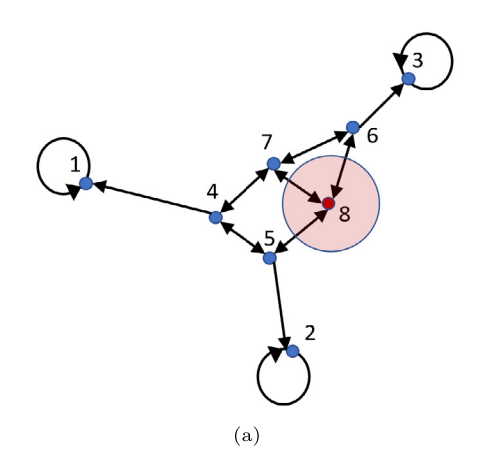
In HDM, the leaders' desired trajectories are given in the form of (1). Therefore, the desired trajectory of the followers can be written as a linear combination of the leaders' desired trajectories as provided in (3). Thus, the desired trajectory of all active UAS can be given by

$$\mathbf{r}_{i,d} = \begin{cases} \mathbf{Q}(t, t_0) \left( \mathbf{r}_{i,0} - \mathbf{d}(t_0) \right) + \mathbf{d}(t) & i \in \mathcal{L} \\ \sum_{j \in \mathcal{L}} \alpha_{i,j} \mathbf{r}_{j,d}(t) & i \in \mathcal{F} \end{cases}$$
 (17)

Because of affinity of the homogeneous deformation coordination, the first and second rows of Eq. (17) are the two (equivalent) forms of homogeneous deformation coordination. The first row of Eq. (17) is same as Eq. (1). Indeed Eq. (1) (the first row of Eq. (17)) enables leaders to plan safe HDM trajectories assuring inter-UAS collision avoidance by constraining the minimum eigenvalue of matrix ( $\mathbf{Q}^T\mathbf{Q}$ ) per Remark 3 of the revised manuscript. The second row of Eq. (17) presents a leader-follower formulation of the homogeneous transformation suitable for followers to acquire the HDM desired trajectories planned by the leaders.

Generation of localization graph. The localization graph is defined or updated at reference time  $t^*$  when HDM starts. At reference time  $t^*$ , all UAS contained in  $\mathcal{C}_0$  are healthy UAS; i.e.  $\mathcal{V}_A(t^*) = \mathcal{V}_H(t^*)$ . The localization graph is defined based on UAS' proximity such that every follower can strictly measure relative positions of k nearest neighbors. Without loss of generality, we choose k=3 and use the Algorithm 1 to generate/update graph  $\mathcal{G}\left(\mathcal{V}_A(t^*), \mathcal{E}\left(t^*\right)\right)$ . Because desired configuration of the MUS is 2-dimensional, we choose three leaders at the boundary of the MUS configuration when HDM is activated and graph  $\mathcal{G}$  is generated. If there exists more that three UAS at the boundary of the MQS configuration, we choose three (out of all boundary UAS) as leaders by using the algorithm provided in [36], and the remaining non-leader boundary UAS are considered as followers.

**Assumption 1.** The topology of localization remains  $\mathcal{G}(\mathcal{V}_A(t^*), \mathcal{E}(t^*))$  time-invariant until HDM is again recovered from FRM.



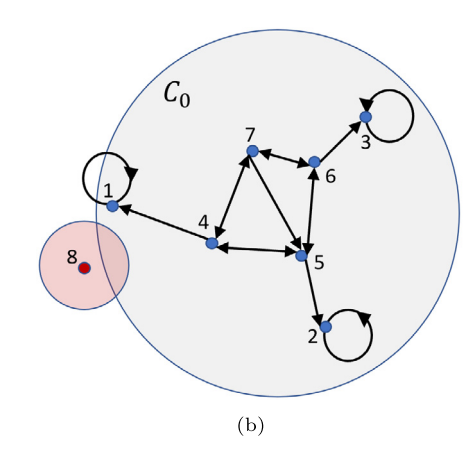


**Fig. 3.** The circular paths indicate that the UAS is able to localize itself in the environment (either using GPS or SLAM). The directional straight arrows between UAS i, j shows that the UAS i is able to calculate  $\mathbf{r}_i(t) - \mathbf{r}_j(t)$  i.e., relative positions of its in-neighbor UAS j. (a) Old localization graph  $\mathcal{G}(\mathcal{V}_A(t), \mathcal{E}(t))$  at time  $t \leq t^*$ . (b) Regeneration of localization graph  $\mathcal{G}(\mathcal{V}_A(t), \mathcal{E}(t))$  at time  $t^*$  when FRM is transitioned to HDM.

Per Assumption 1, the topology of graph  $\mathcal{G}\left(\mathcal{V}_A(t^*), \mathcal{E}\left(t^*\right)\right)$  does not change, if HDM is transitioned to FRM. This implies that any UAS contained by  $\mathcal{C}_0$  can measure and share relative position measurements regardless of the status of healthiness/failure of the contained UAS

Regeneration of localization graph  $\mathcal{G}\left(\mathcal{V}_A(t^*),\mathcal{E}\left(t^*\right)\right)$  takes place when the system has transitioned back to HDM as shown in Fig. 3a. As illustrated, 8 UAS are contained by  $\mathcal{C}_0$  before HDM resumes; UAS 8 is faulty but the remaining UAS are all healthy. At  $t=t^*$ , UAS 8 is outside  $\mathcal{C}_0$ , the operating mode of the system switches from FRM to HDM and the new localization graph is regenerated using Algorithm 1.

**Remark 3.** In HDM, collision avoidance is assured by constraining the eigenvalues of matrix  $\mathbf{U}(t) = (\mathbf{Q}^T(t)\mathbf{Q}(t))^{\frac{1}{2}}$ , denoted by  $\lambda_1$ ,  $\lambda_2$ , and  $\lambda_3$ , to satisfy

$$\bigwedge_{j=1}^{3} \left( \lambda_j(t) \ge \lambda_{min} \right), \qquad j = 1, 2, 3, \ t \ge t_0$$

where  $\lambda_{min}=\frac{\delta+\epsilon}{p_{min}}$  is obtained based on upper bound control error  $\delta$ , UAS size  $\epsilon$ , and minimum separation distance  $p_{min}$  in the reference configuration, at time  $t_0$  when HDM is active [40].

#### Algorithm 1 Network Generating.

```
Input: \mathcal{V}_A(t), \mathcal{L}(t), \mathcal{F}(t), \hat{\mathbf{r}}_i(t), \forall i \in \mathcal{V}_A

Output: \mathcal{G}(\mathcal{V}_A(t), \mathcal{E})

\mathcal{E} = \emptyset
for i \in \mathcal{V}_A do

if i \in \mathcal{L} then

(i,i) \in \mathcal{E}
\mathcal{N}_i = \{i\}
else if i \in \mathcal{F} then

\mathcal{N}_i = 3 — Nearest nodes \in \mathcal{V}_A
(i,j) \in \mathcal{E} \forall j \in \mathcal{N}_i
end if

Generate a graph \mathcal{G}(\mathcal{V}_A, \mathcal{E}) with node set \mathcal{V}_A and edge set \mathcal{E}
end for
```

## 4.2. Coordination planning at FRM

When FRM is active, we use the ideal fluid flow model to plan safety recovery trajectory for every healthy UAS  $i \in \mathcal{V}_H$  such that each UAS safely slides along the stream curve  $\Psi_i = \Psi(x_i(t), y_i(t))$  at any time  $t \geq t^{**}$  when FRM is active, where  $t^{**}$  is the FRM activation time. This leads to excluding every failed UAS from the

motion space by a cylinder elongated in z direction. In order to compute the direction of desired motion for a specific time  $t'>t^{**}$ , we assume that along a stream line, which provides the direction of motion at  $x_i(t')$ ,  $y_i(t')$ , value of  $\Psi$  is constant for all t>t'. Therefore, at time t'

$$\Psi_i = \Psi(x_i, y_i, t') \implies \frac{\partial \Psi}{\partial x} dx + \frac{\partial \Psi}{\partial y} dy = 0$$
 (18)

$$\frac{dy}{dx} = -\frac{\frac{\partial \Psi}{\partial x}}{\frac{\partial \Psi}{\partial y}} \tag{19}$$

From (4),  $\Psi(x_i(t), y_i(t))$  can be written as

$$\Psi(x_i(t), y_i(t)) = \sum_{j \in \mathcal{V}_F} y_i(t) - y_j(t) - \frac{a_j^2(y_i(t) - y_j(t))}{(x_i(t) - x_i(t))^2 + (y_i(t) - y_j(t))^2}.$$
(20)

Substituting the above expression in (19) leads to

$$\frac{dy}{dx} = \sum_{j \in \mathcal{V}_F} \left[ -\frac{2a_j^2(x_i - x_j)(y_i - y_j)}{\Gamma^2 \left( \frac{2a_j^2(y_i - y_j)(y_i - y_j)}{\Gamma^2} - \frac{a_j^2}{\Gamma} + \Gamma \right)} \right]$$
(21)

where 
$$\Gamma = (x_i - x_j)^2 + (y_i - y_j)^2$$
.

In this work, without loss of generality, we suppose that each healthy UAS maintains its speed along x direction. Thus,  $\dot{x}_{i,d}(t)$  is given, and since healthy UAS  $i \in \mathcal{V}_H$  should move along a path with instantaneous slope given by (21),  $\dot{y}_{i,d}(t)$  can be computed in the form of

$$\dot{y}_{i,d}(t) = \dot{x}_{i,d}(t) \times \sum_{j \in \mathcal{V}_F} \left[ -\frac{2a_j^2(x_i - x_j)(y_i - y_j)}{\Gamma^2 \left( \frac{2a_j^2(y_i - y_j)(y_i - y_j)}{\Gamma^2} - \frac{a_j^2}{\Gamma} + \Gamma \right)} \right]. \tag{22}$$

Let  $\Delta t$  denote the time-step for which we want to figure out the desired position of UAS  $i \in \mathcal{V}_H$ . In order to find  $x_{i,d}(t +$ 

 $\Delta t$ ),  $y_{i,d}(t + \Delta t)$ , we can integrate from  $\dot{x}_{i,d}(t)$  and  $\dot{y}_{i,d}(t)$ , respectively. Therefore,

$$x_{i,d}(t+\Delta t) = \int_{t}^{t+\Delta t} \dot{x}_{i,d}(\zeta)d\zeta = x_{i,d}(t) + \dot{x}_{i,d}(t)\Delta t, \qquad (23)$$

$$y_{i,d}(t+\Delta t) = \int_{t}^{t+\Delta t} \dot{y}_{i,d}(\zeta)d\zeta = y_{i,d}(t) + \dot{y}_{i,d}(t)\Delta t.$$
 (24)

Note that we assume healthy UAS move in a plane parallel to x-y plane. That is

$$z_{i,d}(t + \Delta t) = z_{i,d}(t), \quad \dot{z}_{i,d}(t) = 0, \quad \ddot{z}_{i,d}(t) = 0 \quad \forall i \in \mathcal{V}_H.$$
 (25)

In order to find the desired acceleration  $\ddot{x}_{i,d}(t)$ ,  $\ddot{y}_{i,d}(t)$ , we use path curvature in our analysis. Let  $\hat{\mathbf{e}}_{i,t}$  and  $\hat{\mathbf{e}}_{i,n}$  represent the tangential and normal unit vectors at  $x_i(t), y_i(t)$  corresponding to stream line  $\Psi_i$ , respectively. We define  $\theta_i$  as the counter clockwise angle between positive direction of x axis and  $\hat{\mathbf{e}}_{i,t}$ . Therefore,  $\theta_i = \tan^{-1}(\frac{dy_i}{dx_i})$ . Curvature of stream line  $\Psi_i$  at  $x_i(t), y_i(t)$ , denoted by  $\kappa_i$ , can be computed in the following way:

$$\kappa_i = \frac{\frac{d^2 y_i}{dx_i^2}}{\left[1 + \left(\frac{dy_i}{dx_i}\right)^2\right]^{\frac{3}{2}}}$$
(26)

where

$$\frac{d^2 y_i}{dx_i^2} = -\frac{\frac{\partial^2 \Psi}{\partial x^2} \frac{\partial \Psi}{\partial y} - \frac{\partial^2 \Psi}{\partial y^2} \frac{\partial \Psi}{\partial x}}{\left(\frac{\partial \Psi}{\partial y}\right)^2}.$$
 (27)

In the above expression,  $\frac{\partial^2 \Psi}{\partial x^2}$  and  $\frac{\partial^2 \Psi}{\partial y^2}$  can be computed directly from (20). Let  $\mathbf{a}_{i,t}$ ,  $\mathbf{a}_{i,n}$  denote the tangential and normal acceleration along the stream line  $\Psi_i$ , respectively. We assume that each healthy UAS  $i \in \mathcal{V}_H$  moves with zero acceleration along the stream line  $\Psi_i$ . Hence,  $\mathbf{a}_{i,t} = 0$ . Moreover, normal component of the acceleration is

$$\mathbf{a}_{i,n} = (\dot{x}_i^2 + \dot{y}_i^2) \kappa_i \hat{\mathbf{e}}_{i,n}. \tag{28}$$

From the above expression,  $\ddot{x}_{i,d}(t)$  and  $\ddot{y}_{i,d}(t)$  can be computed in the following form

$$\ddot{\mathbf{x}}_{i,d}(t) = |\mathbf{a}_{i,n}| \cos(\theta_i), \tag{29}$$

$$\ddot{y}_{i,d}(t) = |\mathbf{a}_{i,n}| \sin(\theta_i). \tag{30}$$

Using the collective dynamics of (7) and the desired trajectories of each UAS, the multi-UAS (MUS) is enabled to deploy a proper control input to track the desired trajectories.

**Remark 4.** In FRM, collision avoidance is assured by choosing the proper sliding speed along the streamline allocated to each UAS so that the control error upper bound of each healthy UAS does not exceed  $\delta$ 

#### 4.3. Transitions between HDM and FRM

The HDM is transitioned into FRM once a failed UAS is detected. We define error as  $e_i = \|\hat{\mathbf{r}}_i(t) - \mathbf{r}_{i,d}(t)\|$  at time t, where  $\hat{\mathbf{r}}_i(t)$  is

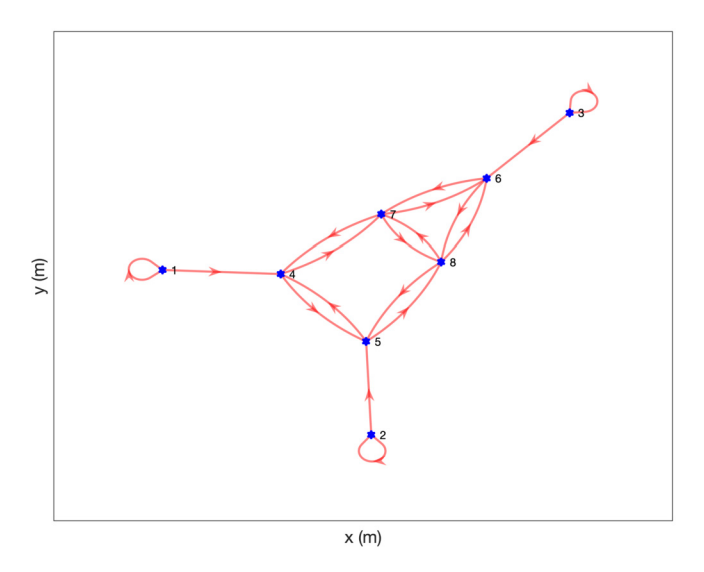


Fig. 4. Initial configuration of the MUS. Leaders 1, 2, 3 are able to localize themselves in the environment.

the estimated global position of UAS  $i \in \mathcal{V}_A$  and  $\mathbf{r}_{i,d}(t)$  is the desired position of UAS i. We consider  $i \in \mathcal{V}_A$  as a failed (active) UAS, when  $e_i(t)$  exceeds a predefined threshold value  $\delta$ . Therefore, FRM is commanded if the following condition holds:

$$\bigvee_{i \in \mathcal{V}} (e_i(t) > \delta), \qquad \forall t, \tag{31}$$

where symbol  $\bigvee$  implies "at least one". Using the above criterion, the commander UAS triggers  $\sigma$  to jump from 1 to 2 when (31) is satisfied (we denote this trigger time by  $t^{**}$ ), and consequently, the system switches to FRM. All healthy UAS in  $\mathcal{V}_H = \mathcal{V}_A \setminus \mathcal{V}_F$  should update their desired trajectories according to the position of failed UAS. Note that  $\mathcal{V}_F(t)$  is defined based only on those UAS which are contained in  $\mathcal{C}_0$ . Further, failed UAS  $i \in \mathcal{V}_F$  is not necessarily static. Algorithm 2 presents the failure detection algorithm used in our paper.

## Algorithm 2 Failure Detection Algorithm.

```
Input: \mathcal{V}_A(t), \mathbf{r}_{i,d}(t), \hat{\mathbf{r}}_{i,d}(t) \forall i \in \mathcal{V}_A
Output: \mathcal{V}_F(t), \sigma(t)
\mathcal{V}_F = \emptyset
for i = 1 : n_a do
e_i(t) = \|\hat{\mathbf{r}}_i(t) - \mathbf{r}_{i,d}(t)\|
if e_i(t) \ge \delta then
\mathcal{V}_F = \{i\} \bigcup \mathcal{V}_F
\sigma = 1
end if
end for
```

Note that FRM is transitioned to HDM once all UAS enclosed by  $\mathcal{C}_0$  are healthy. Therefore, HDM is active if

$$V_H(t) = V_A(t) \tag{32}$$

at time t.

#### 5. Simulation results

In our simulations, we consider a group of 8 UAS in 3-D airspace where each UAS is a quadcopter equipped with proprioceptive sensors. We use the model and trajectory control developed in [41] to obtain the MUS dynamics (7), where  $k_{1,i} = 10$ ,  $k_{2,i} = 35$ ,  $k_{3,i} = 50$ , and  $k_{4,i} = 24$  for every quadcopter UAS  $i \in \mathcal{V}_H$ 

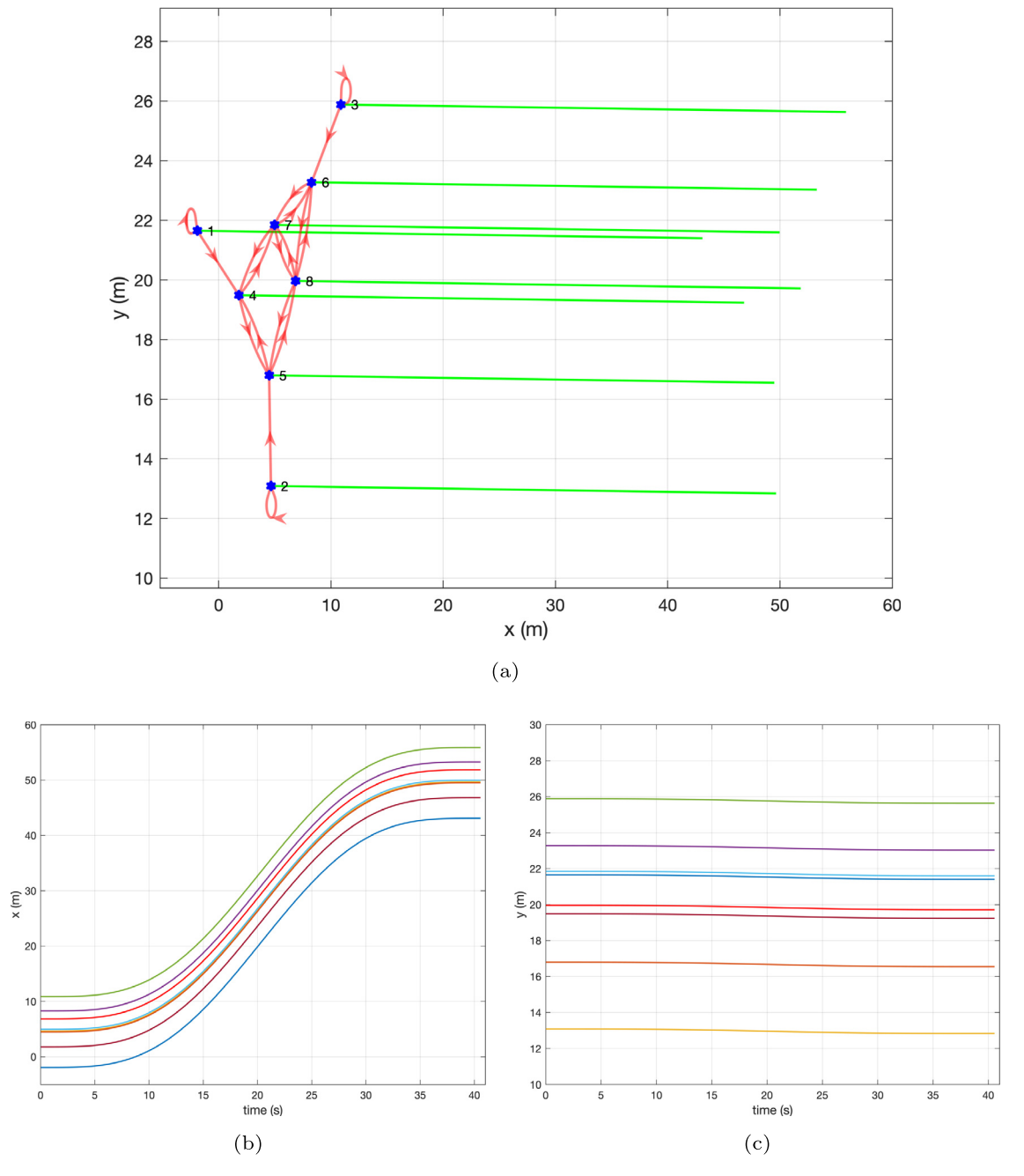


Fig. 5. (a) Initial desired paths of MUS at HDM when all UAS are healthy. (b) x component of desired trajectory of MUS. (c) y component of desired trajectory of MUS.

 $(k_{1,i} \text{ through } k_{4,i} \text{ are defined in Ref. [41]})$ . We consider the covariance of  $10^{-3}$  for process noise  $\eta_i$  and measurement noise  $\epsilon_i$ . Sampling time in our simulations is  $\Delta t = 0.01$  sec.

We assume that all UAS are located at the altitude of 20 m (i.e. z=20 m), and desired altitude is also  $z_d=20$  m. In other words, UAS only move in a plane parallel to x-y plane at z=20 m. The initial configuration of the MUS in x-y plane is shown in Fig. 4. Arrows in Fig. 4 represents the graph  $\mathcal{G}(\mathcal{V}_A,\mathcal{E})$  at initial time. Note that graph  $\mathcal{G}(\mathcal{V}_A,\mathcal{E})$  is a proximity time-varying graph at each node. Initially, MUS is in HDM and all UAS are active and healthy. Hence,  $\mathcal{V}_F=\emptyset$  and  $\mathcal{V}_A=\mathcal{V}_H=\{1,\dots,8\}$ . We label the UAS such that  $\mathcal{L}=\{1,2,3\}$  and  $\mathcal{F}=\{4,\dots,8\}$ . When the MUS is at HDM, the desired trajectories of the leaders and followers are computed based on (1) and (3), respectively. Fig. 5a shows the initial desired path of all UAS when MUS is in HDM and all UAS are

healthy. Fig. 5b and 5c show the x and y components of the desired trajectories of all UAS, respectively.

## 5.1. A group of 8 UAS with multiple static failed UAS

Consider a scenario in which two UAS are subjected to actuation failures at predefined times  $t^{**}=10\,\mathrm{sec}$  and  $t_2=15\,\mathrm{sec}$ . In order to simulate the failure in the MUS, we deploy an external control on UAS 8, 7 to stop at  $t^{**}=10\,\mathrm{sec}$  and  $t_2=15\,\mathrm{sec}$ , respectively. Using the Algorithm 2 and considering  $\delta=0.5$ , UAS 8 is detected as a failed UAS in the MUS at  $t_1'=10.64\,\mathrm{sec}$ . Fig. 6a shows the trajectories of UAS from  $t_0=0$  to  $t_1'=10.64\,\mathrm{sec}$ . In Fig. 6, blue and green lines correspond to the actual and desired trajectories in x-y plane, respectively. Also, green and red star correspond to healthy and failed UAS in Fig. 6, respectively. Moreover, unsafe zone corresponding to the failure of UAS is shown by a circular

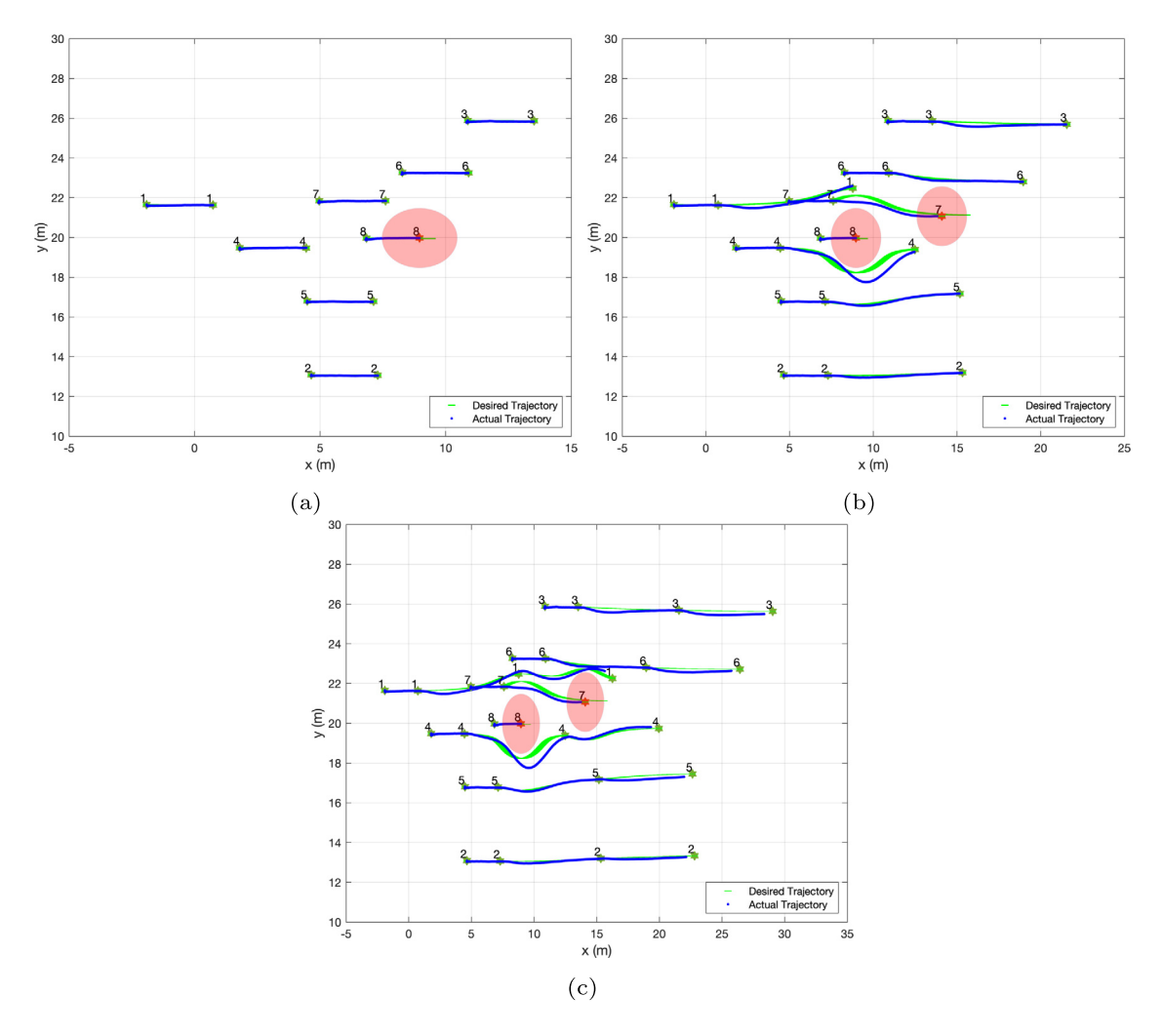


**Fig. 6.** Desired and actual paths. Red circles are the unsafe-zone corresponding to each failure. (a) Paths before failure at  $t^{**}$ . (b) Paths before failure at  $t_2$ . (c) Paths before switching to HDM.

area with radius of a = 1.5 m. At  $t'_1 = 10.64$  sec, FRM is activated and the system is switched to FRM. In this mode, desired trajectories of the MUS are computed based on the approach explained in Section 4.2. Actual paths of all healthy UAS are shown in Fig. 6. As shown in this figure, all UAS modify their desired trajectories to wrap the failed UAS 8 and avoid collision in the system. We deploy a second failure in the system at  $t_2 = 15 \,\mathrm{sec}$ , which is detected automatically at  $t_2' = 15.54$  sec. Note that system maintains the underlying graph till the operating mode is switched. After the second failure, system is still in FRM till all 6 healthy UAS pass the failed UAS 7, 8. This condition is satisfied at  $t_3 = 17.86 \,\mathrm{sec}$ . Fig. 6c shows the path of all UAS for  $t < t_3$ . At  $t_3 = 17.86$  sec the commander UAS decides to switch the system to HDM, and consequently, a new coordination graph is generated at this time and new desired trajectories are constructed for all 6 healthy UAS. As shown in Fig. 7, at  $t_3 = 17.86$  sec, underlying graph  $\mathcal{G}(\mathcal{V}_A, \mathcal{E})$  has been updated. Fig. 7 shows the trajectories of all UAS in two different modes in x - y plane. Fig. 8a and 8b show the x and y components of the actual trajectories of all UAS in each mode.

#### 5.2. A group of 8 UAS with 1 time-varying failed UAS

In these simulations, we consider the scenario where a single UAS is subjected to failure at  $t^{**} = 10 \, \text{sec}$  and then moves at a constant velocity in a random direction. We have presented results where the failed UAS moves in 1-D for some time  $t'_*$ , but our approach can be extended to multiple directions. Figs. 9a, 10a

shows the trajectories of UAS from  $t_0$  to  $t'_1$  where  $t'_1$  is the time at which failure is detected. Blue dots and green lines correspond to the actual and desired trajectories in x - y plane, respectively, whereas green and red star correspond to healthy and failed UAS, respectively. The unsafe zone is represented as a circular area with radius of a = 1.5 m which corresponds to failure of UAS 8 and 7 in Figs. 9a, 10a respectively. FRM is activated at  $t'_1$  and the desired trajectories of the MUS are computed based on the approach explained in Section 4.2. However in each case, the failed UAS is also moving at a constant velocity in a particular direction i.e., negative x direction when UAS 8 fails and positive y direction when UAS 7 fails. We can observe in Figs. 9b, 10b that all healthy UAS modify their desired trajectories to wrap the failed UAS when the failed UAS is moving at constant velocity and avoid collision with the failed UAS and other healthy UAS. At  $t_2$ , after all the healthy UAS have passed the failed UAS, the system switches back to HDM, and consequently, a new coordination graph will be generated at this time and new desired trajectories are constructed for all 7 healthy UAS. The table below shows the different times at which the failures are detected, and the system switches back to HDM.

| Experiment | Failed UAS | $t_0$ sec | $t_1'$ sec | $t_2$ sec | $t'_*$ sec |
|------------|------------|-----------|------------|-----------|------------|
| 1          | 8          | 0         | 10.4       | 17.3      | 0.5        |
| 2          | 7          | 0         | 10.2       | 15.7      | 2          |

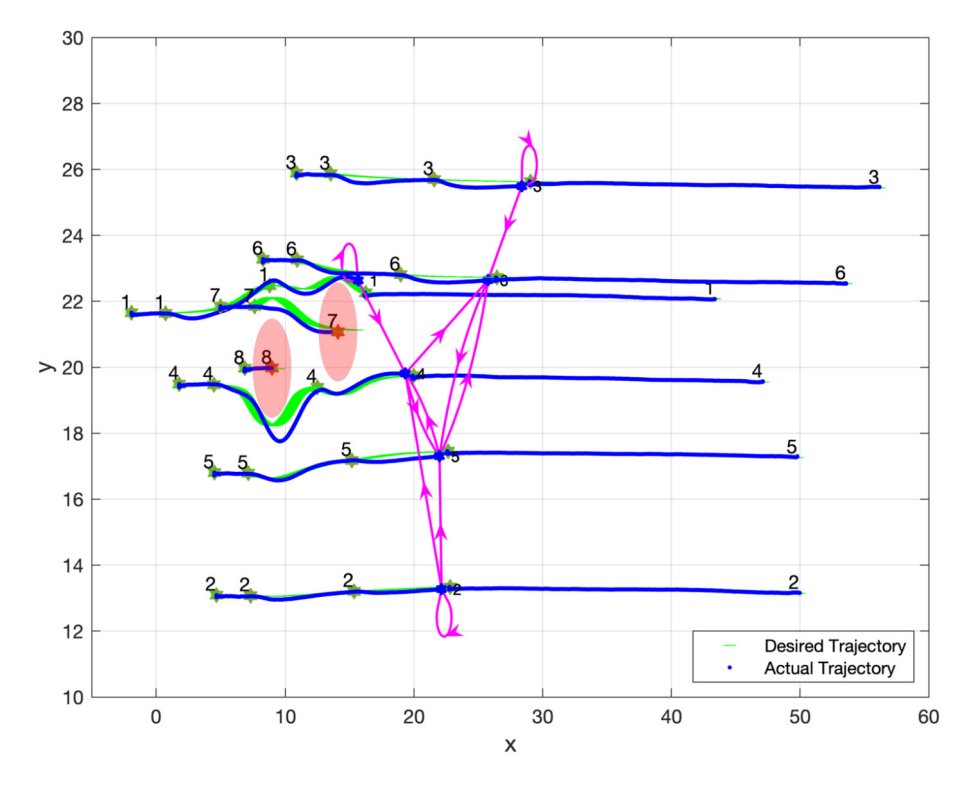


Fig. 7. Green lines are desired trajectories and blue lines are actual trajectories of UAS. Updated  $\mathcal{G}(\mathcal{V}_A, \mathcal{E})$  is shown when system is switched to HDM after FRM.

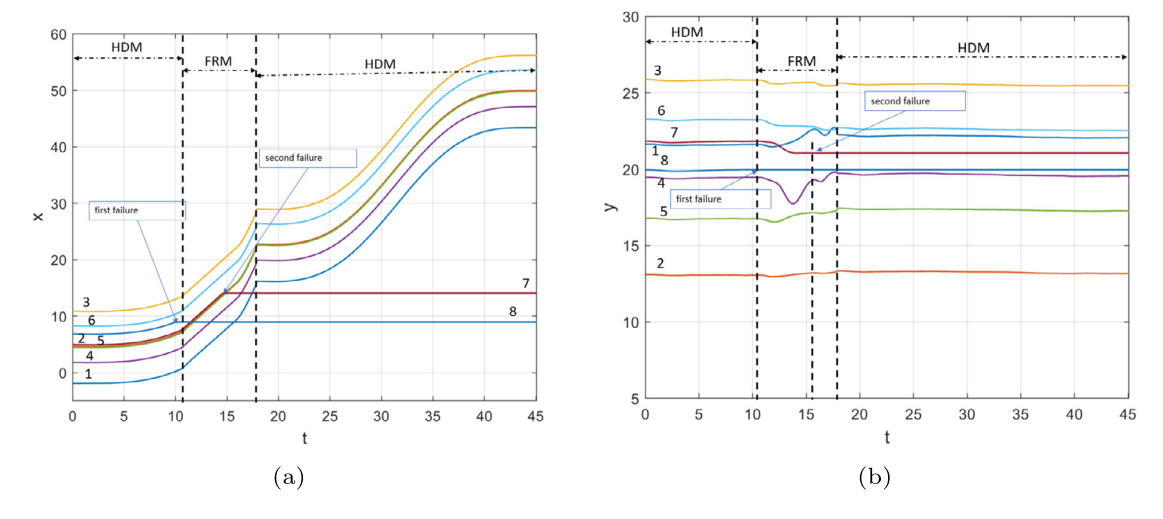


Fig. 8. (a) x and (b) y components of actual trajectories of all UAS.

## 6. Conclusion, discussion, and future work

This paper presents a novel approach for fault-resilient multi-UAS coordination in the presence of abrupt and unpredictable UAS failure. We applied the principles of continuum mechanics to enforce safety of the multi-UAS coordination and specify the conditions for transitions between Homogeneous Deformation Mode (HDM) and Fault Resilient Mode (FRM) and vice versa. We also applied the Cooperative Localization approach to detect the failed UAS and localize healthy UAS with respect to the global coordinate system at low computational cost. We have also accounted for multiple UAS failures in the MUS and the conditions for switching between HDM and FRM in such a case. Our approach was validated through simulations by successfully conducting experiments on two different sets of failures: (1) with multiple static UAS failure in the MUS, and (2) with a single time-varying UAS failure in the MUS. A drawback of this approach is that we consider actu-

ation failure and assume that the sensors for the failed UAS are functioning. Future works in this area would be to account for this drawback and further develop a data-driven approach by leveraging the principles of continuum mechanics to guarantee safety.

### **Declaration of competing interest**

The corresponding author (the project PI) declares that they have no known competing financial interests or personal relationships that could have appeared to influence the work reported in this paper.

## Acknowledgement

This work has been supported by the National Science Foundation under Award Nos. 2133690 and 1914581.

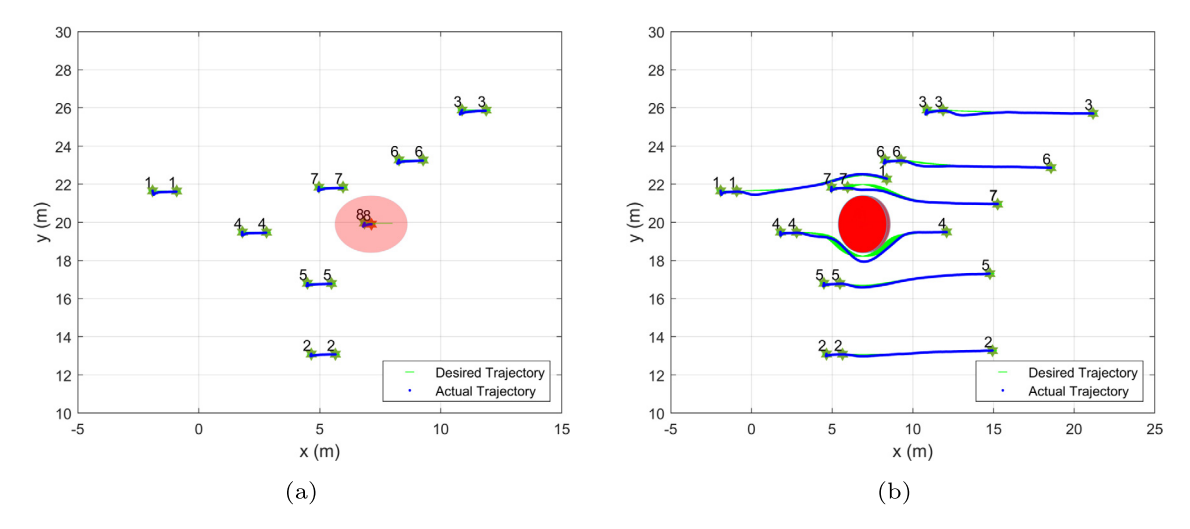


Fig. 9. Desired and actual paths. Red circle is the unsafe-zone corresponding to UAS failure 8. (a) Paths before failure at  $t^{**}$ . (b) Paths after the system switched from FRM to HDM.

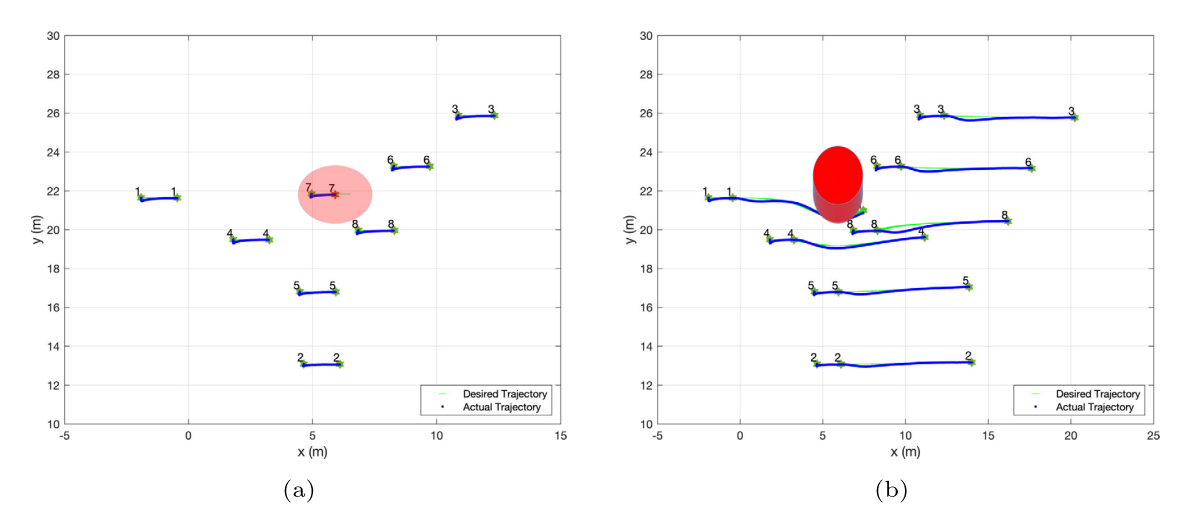


Fig. 10. Desired and actual trajectories. Red circle is the unsafe-zone corresponding to failed UAS 7. (a) Trajectories before failure at  $t^{**}$ . (b) Trajectories after the system switched from FRM to HDM.

#### References

- [1] S. Jung, H. Kim, Analysis of Amazon prime air UAV delivery service, J. Knowl. Inform. Technol. Syst. 12 (2) (2017) 253–266.
- [2] T. Kersnovski, F. Gonzalez, K. Morton, A UAV system for autonomous target detection and gas sensing, in: 2017 IEEE Aerospace Conference, IEEE, 2017, pp. 1–12.
- [3] B. Argrow, D. Lawrence, E. Rasmussen, UAV systems for sensor dispersal, telemetry, and visualization in hazardous environments, in: 43rd AIAA Aerospace Sciences Meeting and Exhibit, 2005, p. 1237.
- [4] D.C. Tsouros, S. Bibi, P.G. Sarigiannidis, A review on UAV-based applications for precision agriculture, Information 10 (11) (2019) 349.
- [5] E. Semsch, M. Jakob, D. Pavlicek, M. Pechoucek, Autonomous UAV surveillance in complex urban environments, in: 2009 IEEE/WIC/ACM International Joint Conference on Web Intelligence and Intelligent Agent Technology, vol. 2, IEEE, 2009, pp. 82–85.
- [6] H. Haghighi, D. Asadi, D. Delahaye, Multi-objective cooperated path planning of multiple unmanned aerial vehicles based on revisit time, J. Aerosp. Inform. Syst. 18 (12) (2021) 919–932.
- [7] H. Surmann, R. Worst, T. Buschmann, A. Leinweber, A. Schmitz, G. Senkowski, N. Goddemeier, Integration of UAVs in urban search and rescue missions, in: 2019 IEEE International Symposium on Safety, Security, and Rescue Robotics (SSRR), IEEE, 2019, pp. 203–209.
- [8] J. Witczuk, S. Pagacz, A. Zmarz, M. Cypel, Exploring the feasibility of unmanned aerial vehicles and thermal imaging for ungulate surveys in forests-preliminary results, Int. J. Remote Sens. 39 (15–16) (2018) 5504–5521.
- [9] E.V. Butilă, R.G. Boboc, Urban traffic monitoring and analysis using unmanned aerial vehicles (UAVs): a systematic literature review, Remote Sens. 14 (3) (2022) 620.

- [10] D. Liu, W. Bao, X. Zhu, B. Fei, Z. Xiao, T. Men, Vision-aware air-ground cooperative target localization for UAV and UGV, Aerosp. Sci. Technol. 124 (2022) 107525
- [11] J. Kwak, Y. Sung, Autonomous UAV flight control for GPS-based navigation, IEEE Access 6 (2018) 37947–37955.
- [12] H. Lu, H. Shen, B. Tian, X. Zhang, Z. Yang, Q. Zong, Flight in GPS-denied environment: autonomous navigation system for micro-aerial vehicle, Aerosp. Sci. Technol. 124 (2022) 107521.
- [13] R. Li, J. Liu, L. Zhang, Y. Hang, LIDAR/MEMS IMU integrated navigation (SLAM) method for a small UAV in indoor environments, in: 2014 DGON Inertial Sensors and Systems (ISS), IEEE, 2014, pp. 1–15.
- [14] J.J. Leonard, H.F. Durrant-Whyte, Mobile robot localization by tracking geometric beacons, IEEE Trans. Robot. Autom. 7 (3) (1991) 376–382.
- [15] J. Farlik, M. Kratky, J. Casar, Detectability and jamming of small UAVs by commercially available low-cost means, in: 2016 International Conference on Communications (COMM), IEEE, 2016, pp. 327–330.
- [16] S.S. Kia, S. Rounds, Sonia Martinez, Cooperative localization for mobile agents, IEEE Control Syst. Mag. 36 (2) (2016) 86–101.
- [17] A. Chakraborty, R. Sharma, K. Brink, Cooperative localization for multi-rotor UAVs, in: AIAA Scitech 2019 Forum, 2019, p. 0684.
- [18] E.D. Nerurkar, S.I. Roumeliotis, A. Martinelli, Distributed maximum a posteriori estimation for multi-robot cooperative localization, in: 2009 IEEE International Conference on Robotics and Automation, IEEE, 2009, pp. 1402–1409.
- [19] Y. Li, C. Tang, K. Li, S. Peeta, X. He, Y. Wang, Nonlinear finite-time consensus-based connected vehicle platoon control under fixed and switching communication topologies, Transp. Res., Part C, Emerg. Technol. 93 (2018) 525–543.
- [20] X. Yang, S. Song, Three-dimensional consensus algorithm for nonsingular distributed cooperative guidance strategy, Aerosp. Sci. Technol. 118 (2021) 106958.

- [21] Y. Cao, W. Ren, M. Egerstedt, Distributed containment control with multiple stationary or dynamic leaders in fixed and switching directed networks, Automatica 48 (8) (2012) 1586–1597.
- [22] J. Kim, K.-D. Kim, V. Natarajan, S.D. Kelly, J. Bentsman, PdE-based model reference adaptive control of uncertain heterogeneous multiagent networks, Nonlinear Anal. Hybrid Syst. 2 (4) (2008) 1152–1167.
- [23] H. Rastgoftar, Continuum Deformation of Multi-Agent Systems, Springer, 2016.
- [24] H. Rastgoftar, E.M. Atkins, Cooperative aerial lift and manipulation (CALM), Aerosp. Sci. Technol. 82 (2018) 105–118.
- [25] H. Emadi, H. Uppaluru, H. Rastgoftar, A physics-based safety recovery approach for fault-resilient multi-quadcopter coordination, arXiv preprint, arXiv: 2110.07777.
- [26] L. Wang, Q. Guo, Distance-based formation stabilization and flocking control for distributed multi-agent systems, in: 2018 IEEE International Conference on Mechatronics and Automation (ICMA), IEEE, 2018, pp. 1580–1585.
- [27] S.S. Kia, J. Hechtbauer, D. Gogokhiya, S. Martinez, Server-assisted distributed cooperative localization over unreliable communication links, IEEE Trans. Robot. 34 (5) (2018) 1392–1399.
- [28] S.I. Roumeliotis, G.A. Bekey, Distributed multirobot localization, IEEE Trans. Robot. Autom. 18 (5) (2002) 781–795.
- [29] A. Howard, M.J. Matarić, G.S. Sukhatme, Mobile sensor network deployment using potential fields: a distributed, scalable solution to the area coverage problem, in: Distributed Autonomous Robotic Systems 5, Springer, 2002, pp. 299–308.
- [30] A. Prorok, A. Martinoli, A reciprocal sampling algorithm for lightweight distributed multi-robot localization, in: 2011 IEEE/RSJ International Conference on Intelligent Robots and Systems, IEEE, 2011, pp. 3241–3247.
- [31] J.-O. Nilsson, D. Zachariah, I. Skog, P. Händel, Cooperative localization by dual foot-mounted inertial sensors and inter-agent ranging, EURASIP J. Adv. Signal Process, 2013 (1) (2013) 1–17.

- [32] S. Ramasamy, R. Sabatini, A. Gardi, J. Liu, Lidar obstacle warning and avoidance system for unmanned aerial vehicle sense-and-avoid, Aerosp. Sci. Technol. 55 (2016) 344–358.
- [33] C. Kang, J. Davis, C.A. Woolsey, S. Choi, Sense and avoid based on visual pose estimation for small UAS, in: 2017 IEEE/RSJ International Conference on Intelligent Robots and Systems (IROS), IEEE, 2017, pp. 3473–3478.
- [34] S. Ramasamy, R. Sabatini, A unified approach to cooperative and non-cooperative sense-and-avoid, in: 2015 International Conference on Unmanned Aircraft Systems (ICUAS), IEEE, 2015, pp. 765–773.
- [35] X. Yu, Y. Zhang, Sense and avoid technologies with applications to unmanned aircraft systems: review and prospects, Prog. Aerosp. Sci. 74 (2015) 152–166.
- [36] H. Rastgoftar, Fault-resilient continuum deformation coordination, IEEE Trans. Control Netw. Syst. 8 (1) (2020) 423–436.
- [37] H. Rastgoftar, E.M. Atkins, D. Panagou, Safe multiquadcopter system continuum deformation over moving frames, IEEE Trans. Control Netw. Syst. 6 (2) (2018) 737–749
- [38] H. Rastgoftar, E. Atkins, Physics-based freely scalable continuum deformation for UAS traffic coordination, IEEE Trans. Control Netw. Syst. 7 (2) (2019) 532–544.
- [39] D. Simon, Optimal State Estimation: Kalman, H Infinity, and Nonlinear Approaches, John Wiley & Sons, 2006.
- [40] H. Rastgoftar, I.V. Kolmanovsky, A spatio-temporal reference trajectory planner approach to collision-free continuum deformation coordination, Automatica 142 (2022) 110255.
- [41] H. Rastgoftar, I.V. Kolmanovsky, Safe affine transformation-based guidance of a large-scale multi-quadcopter system (MQS), IEEE Trans. Control Netw. Syst. (2021) 1, https://doi.org/10.1109/TCNS.2021.3084038.